The nature and suppression strategies of interfacial reactions in all-solid-state batteries

Fucheng Ren,[a] Ziteng liang,[b] Wengao Zhao,[c] Wenhua Zuo,[d] Min Lin,[b] Yuqi Wu,[a] Xuerui Yang,[a] Zhengliang Gong,[*a] and Yong Yang[*a, b]

[a] College of Energy, Xiamen University, Xiamen 361102, China. E-mail: yyang@xmu.edu.cn

[b] State Key Laboratory for Physical Chemistry of Solid Surface, Department of Chemistry, College of Chemistry and Chemical Engineering, Xiamen University, Xiamen, 361005, China

[c] Institute of Nanotechnology, Karlsruhe Institute of Technology (KIT), 76344 Eggenstein-Leopoldshafen, Germany

[d] Chemical Sciences and Engineering Division, Argonne National Laboratory, Lemont, IL, 60439, USA

Interface stability

The Chemical Stability between sulfide solid electrolytes (SSEs) and cathode/coating was estimated by the thermodynamic approximation method. The SSEs-cathode/coating interface can be assumed as a pseudo-binary system (A: SSEs, B: cathode/coating), equation 1.

$$C_{interface}(c_A,c_B) = \mathrm{x}\, c_A + (1-x)c_B \qquad \textbf{(1)}$$

Where x is the molar fraction of SSEs, and c_A and c_B are the specific composition of SSEs and cathode/coating. The total energy of pseudo-binary interface is described as the liner combination of SSE and cathode/coating, equation 2. $E(c_A)$ and $E(c_B)$ are the ground state energy of SSE and cathode/coating, respectively.

$$\Delta E_{interface}(c_A,c_B,x) = \mathrm{x}\, E(c_A) + (1-x)E(c_B) \qquad \textbf{(2)}$$

The mutual reaction energy $\Delta E_{D,mutual}(c_A,c_B,x)$ can be calculated by constructing a pseudo-binary phase diagram between SSE and cathode/coating and determining the ratio (x) that result in the most negative mutual reaction energy, equation 3:

$$\Delta E_{D,mutual}(c_A,c_B,x) = \min_{x\in[0,1]} \frac{1}{N}[E_{eq,\ interface}(xc_A + (1-x)c_B) - xE_D(c_A) - (1-x)E_D(c_B)]$$

(3)

Here, $E_{eq,\ interface}$ is the reaction energy of the pseudo-binary phase, $E_D(c_A)$ and $E_D(c_B)$ are the decomposition energy of SSE and cathode/coating. N is the number of atoms involved in the phase equilibrium used to normalization.

The Electrochemical Stability of the SSE/cathode interface was evaluated by inducing the extra applied Li chemical potential $\mu_{Li}^{open,\emptyset}$:

$$\mu_{Li}^{open,\emptyset} = \mu_{Li}^{0} - e\emptyset \qquad \textbf{(4)}$$

μ_{Li}^{0} and $\emptyset$ are chemical potential of Li metal and the applied potential referenced to Li metal.

The mutual electrochemical reaction energy $\Delta E_{D,\,mutual}^{\emptyset}(c_A,c_B,x,\emptyset)$ between SSE and cathode can be calculated by the following equation:

$$\Delta E_{D,\,mutual}^{\emptyset}(c_A,c_B,x,\emptyset) = \min_{x\in[0,1]} \frac{1}{N_{gc}}[E_{eq}^{\emptyset}(xc_A + (1-x)c_B) - xE_D^{\emptyset}(c_A) - (1-x)E_D^{\emptyset}(c_B)]$$

(5)

It should be noted that the normalization factor N_{gc} in eq 5, unlike N in eq 3, is the total number of atoms excluding Li.

The applied chemical potential of μ_{Li} at fully ($\mu_{Li}^{open,F}$) and half ($\mu_{Li}^{open,H}$) lithiated state of specific cathode materials are different from each other and determined by calculating the Li chemical window of each cathode at fully and half lithiated state shown in Fig S2a. $\mu_{Li}^{open,F}$ refers to the lowest

chemical potential (corresponding to the highest applied voltage) that the fully-lithiated cathode would not be reduced and $\mu_{Li}^{open,H}$ refers to the highest chemical potential (corresponding to the lowest applied voltage) that half-lithiated cathode would not be oxidized. The specific value of $\mu_{Li}^{open,F}$ and $\mu_{Li}^{open,H}$ for each cathode is listed in Fig. S2b.

Conductivity of interphase layer

The electronic conductivity of the interface layer greatly influences the cyclability of ASSBs. Experimentally, it is extremely difficult to measure the electronic conductivity of a paper-thin and berried interphase layer between cathode and SSE. By analyzing the phase equilibrium between cathode and sulfide solid electrolytes (SSEs), plenty of transition-metal sulfides (M_xS_y, M: Ni, Co, and Mn) are formed at interface. All these M_xS_y possess zero Kohn-Sham band gap as an electronic conductor in the interphase layer, providing the electron conducting net for electrochemical reaction between cathodes and SSEs. It has been proved that a low band gap almost certainly leads to some electronic conductivity.[1] Hence, the percentage of molar fraction (f) of these electronically conductive species with the Kohn-sham band gap < 0.5 eV in all interphases formed at interface are calculated which can effectively reflect the electronic conductivity of the interphase layer. For $x \in [0,1]$ in **eq 3** and **eq 5**, there are several possible phase equilibriums between SSEs and cathodes/coatings. For example, **table S2** lists all possible phase equilibriums between LCO and Li_3PS_4 at fully/half-lithiated of cathode, as well as at chemical potential of μ_{Li} at fully/half-lithiated state of LCO (corresponding to the applied voltage). **Table S3** lists the Kohn-Sham band gaps of all possible products. For each phase equilibrium between LCO and Li_3PS_4 listed in **table S2**, the percentage of molar fraction **(**f_i**)** of electronically conductive species with the Kohn-sham band gap < 0.5 eV in all products was calculated (excepting Li metal in the electrochemical reaction which can be regarded as plating at anode side). Hence, there is a specific f_i values for each equilibrium (f_1, f_2, ……f_n, n is the number of phase equilibriums listed in **Table S2**) and then an average of f_1, f_2, …… and f_n was performed to obtain the final f as the descriptor to evaluate the electronic conductivity of the interface layer. The bigger f means the better electronic conductivity of interface layer, and the severe electrochemical reactions occur between cathodes and SSEs

Geometric analysis

The transport characteristics of Li-ion are highly correlated to the crystal structures. The crystal space of selected structures can be divided into two aspects: space of atoms and interatomic voids.[2] Since the size of interatomic voids is critical for Li conduction, CVAD (Crystal structure Analysis by Voronoi Decomposition)[3] was used to characterize the void spaces and construct the net of interstices in the immobile framework of selected candidates. This code has been widely used to identify the fast ion conductors.[4-8] The threshold of ion that can pass through a, b and c direction of crystal structure is calculated and listed in **table S7**.

BVSE calculations

The Bond Valence Site Energy (BVSE) model is an effective approach to identify ionic transport channels and calculate the migration energy barrier which is suitable to be used in the high-throughput screening scheme due to its low computational cost.[4, 9, 10] BVSE method is an extension of Bond valence Sum (BVS) method by taking the Morse type potential term for cation-anion pairs and Coulomb repulsions between mobile ion and ions with the same charge sign into consideration. The BVS method is based on the principle of the local electroneutrality that the ion oxidation state should be close to the bond valence sum S_{M-X} defined by the following Equation:[11]

$$S_{M-X} = e^{\frac{R_0 - R}{b}} \quad \textbf{(6)}$$

where R_0 and b are constants depending on the type of ions M and X, R is the distance to the neighbor counter-ion. The transport channels can be identified as positions in the crystal structure with low bond valence mismatch.[12-14] The BVSE model can be described as equation 7

$$BVSE = \frac{D_0}{2}\sum_i \left\{(\exp\left[a(R_{min} - R)\right] - 1)^2 - 1\right\} + \sum_{i-1}^{N} E_{coulomb}(M - M_i) \quad \textbf{(7)}$$

Where D_0, a and R_{min} are Morse potential parameters determined from plenty of stable compounds. The Morse bond breaking energy of the same interaction in the energy landscapes of M and $M_i$would be double calculated, $\frac{D_0}{2}$ was used as a simple average method to prevent overestimating the migration. The Coulomb repulsions between two different cations in equation 7 are calculated by the following equation:

$$E_{coulomb}(M - M_i) = \frac{q_M q_{M_i}}{R_{M-M_i}} erfc\left[\frac{R_{M-M_i}}{f\left(r_M - r_{M_i}\right)}\right] \quad \textbf{(8)}$$

Where q is the fractional charge of the interacting ions (M and M_i), R is the bond distance between M and M_i, $erfc(x)$ is a complementary error function which has advantage of fast convergence compared with $\frac{1}{R}$ coulombic interaction, r refers to the covalent radius of the atom, and the screening factor f is set to be 0.74 refers to an empirical quantity. By default, we set the cutoff radius for calculating the interactions to be 10 Å and 0.1 Å as the grid resolution.

Cell assembly and electrochemical characterization

Single crystal NCM811 without any modification treatment was mixed with LPS/LGPS/LPSCl (weight ratio: 7:3) by ball milling at 200 rpm for 1h as cathode materials. 100 mg LPS/LGPS/LPSCl was firstly pressed at 30 MPa to obtain SSEs layer, and the cathode composite was put on the one side. A piece of Li-In was put on the other side as anode. Finally, the cell was pressed at 600 MPa to ensure tight contact. During cycling, 50 MPa pressure was applied to the cell. The battery was tested with LAND CT-2001A (Wuhan, China) test system within 2.4 – 3.7 V vs. Li^+/LiIn at different rate (1C = 200 mA g^{-1}) under room temperature (RT). The current density of the first three cycles is set to be cycled at 0.1 C and then increase to 0.3 C for testing the cycle performance of cells assembled with different composite cathodes (NCM811-LPS/LGPS/LPSCl)

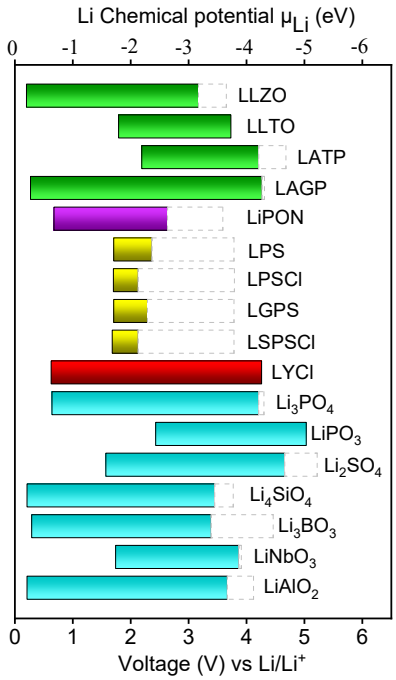

Fig. S1 Electrochemical stability window of SSEs and coating commonly used at cathode side. The oxidation potential to fully delithiated the material is marked by the dashed line.

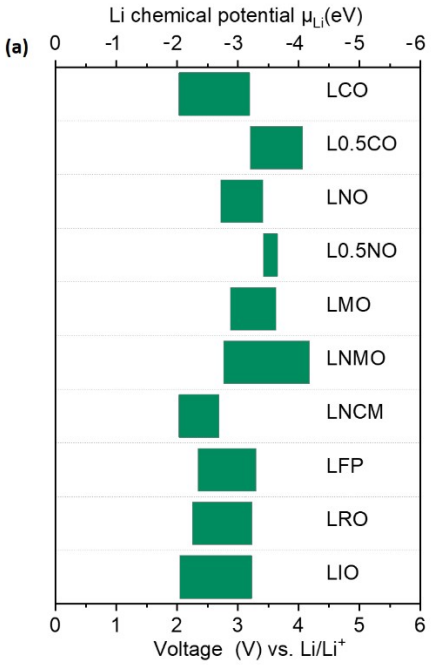

(b)

	$\mu_{Li}^{open,F}$	$\mu_{Li}^{open,H}$
LCO	-2.03	-4.08
LNO	-2.72	-3.42
LMO	-2.88	-3.65
LNMO	-2.76	-4.19
LNCM	-2.03	-3.66
LFP	-2.34	-3.36
LRO	-2.25	-3.23
LIO	-2.04	-3.24

Fig. S2 Li chemical window of common cathodes (a), and applied chemical potential in fully ($\mu_{Li}^{open,F}$) and half ($\mu_{Li}^{open,H}$) lithiated of cathode (b).

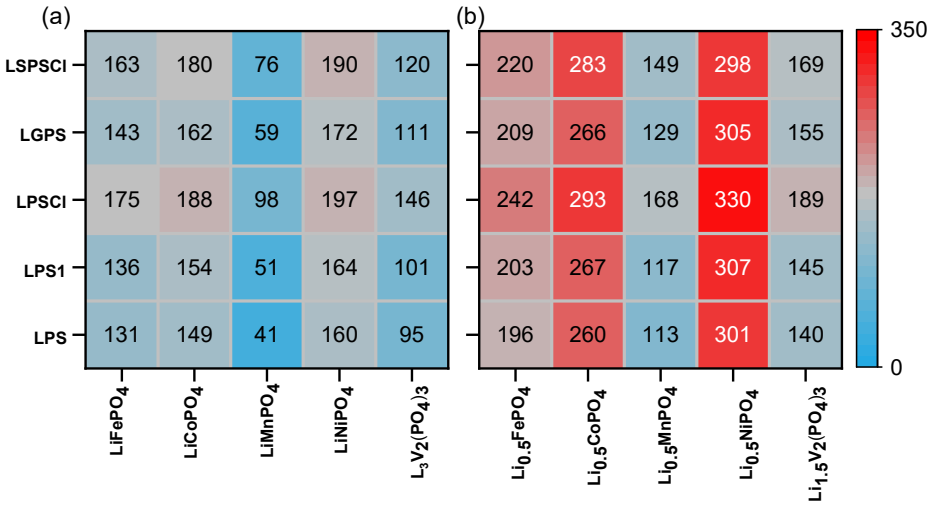

Fig. S3 Chemical compatibility between polyanion cathodes and SSEs with the largest magnitude of chemical reaction energies ($^{-}\Delta E_{D,mutual}$) of polyanion cathodes /SSEs interface in meV/atom. Chemical reaction energy in fully (a) and half lithiated state of cathodes (b).

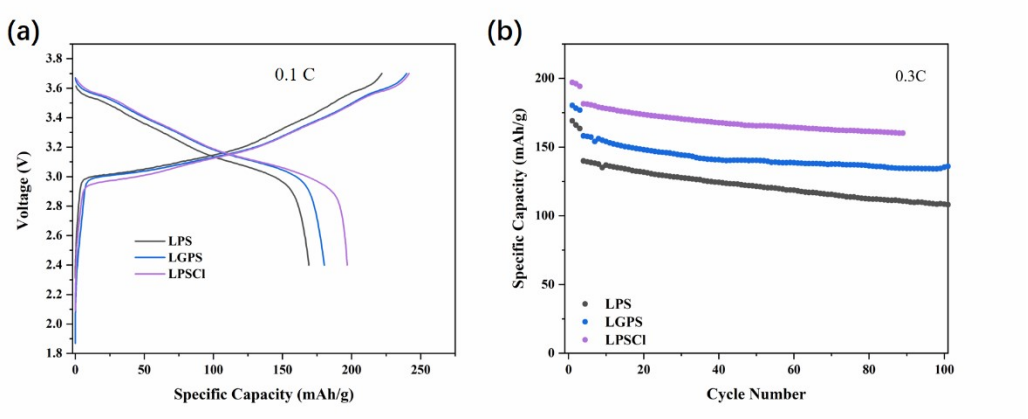

Fig. S4 (a) The first charge and discharge curves of cells assembled with different composite cathodes NCM-LPS/LGPS/LPSCl at 0.1C (20 mA g^{-1}). (b) Cycle performance of the first 100 cycles at 0.3 C (60 mA g^{-1}).

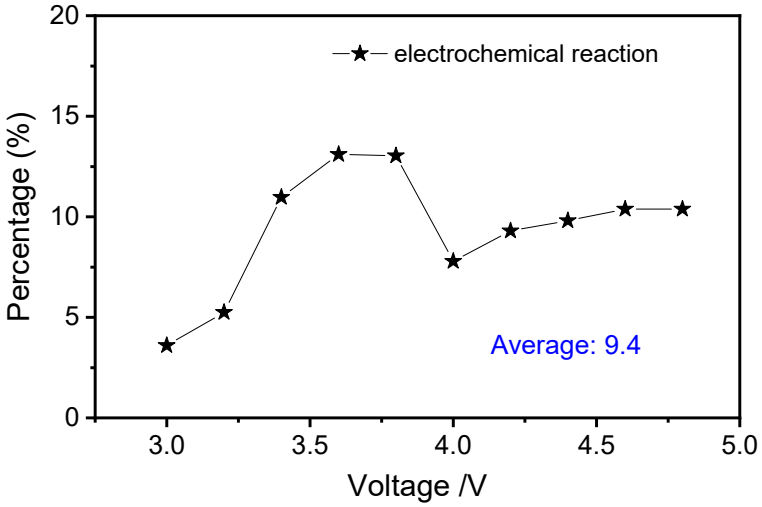

Fig. S5 Percentage of molar fraction of the species with the Kohn-Sham band gap smaller than 0.5 eV in all interphases formed by the electrochemical reaction between $LiNi_{0.5}Mn_{1.5}O_4$ and $LiPO_2N$.

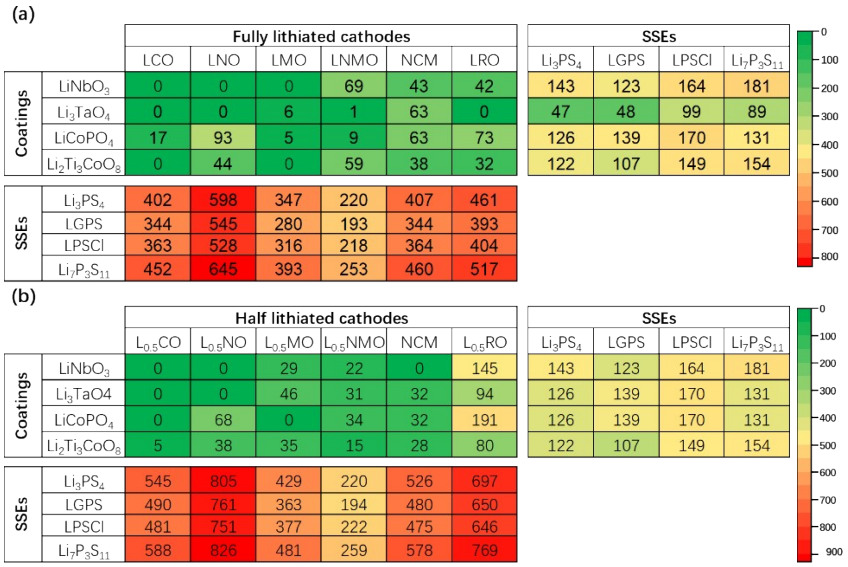

Fig. S6 Chemical reaction energies ($^{-}\Delta E_{D,mutual}$) of cathodes/SSEs and cathodes/coatings in fully (a) and half (b) lithiated state of cathode and coatings/SSEs.

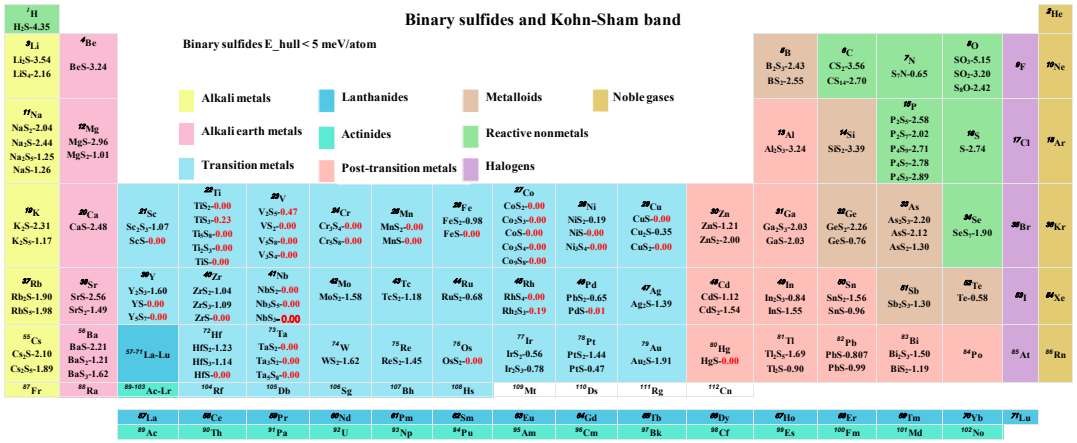

Fig. S7 The schematic of Kohn-sham band gap of binary sulfides throughout the whole Periodic Table. The corresponding binary sulfides of each element are listed below the element symbol and the band gap are followed behind the line.

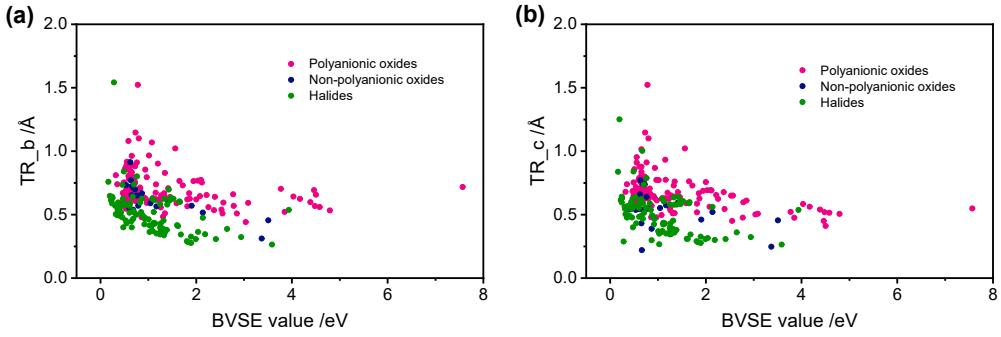

Fig. S8 Threshold size and BVSE values of candidates pass the filter 4 along (a) b and (b) c direction of the structure.

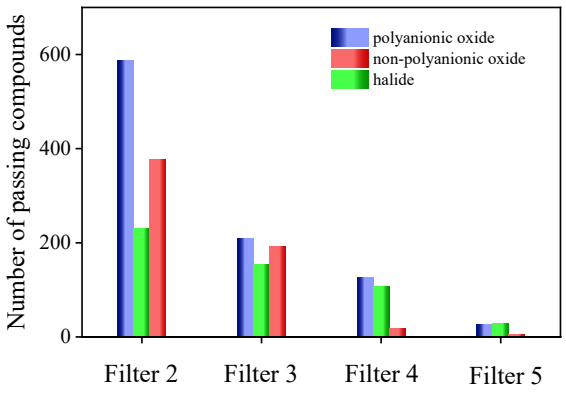

Fig. S9 Histogram of numbers of compounds for each category that pass each filter in the high-throughput screening. Red, blue, and green color indicates the non-polyanionic oxides, polyanionic oxides, and halide, respectively. Filter 2-5 corresponding to phase stability, excluding the elements trends to form electronically conductive interphase, chemical stability with Li_6PS_5Cl and NCM, and fast Li ion conductivity.

Table S1. Oxidation products of sulfide electrolytes in fully-delithiated state.

Electrolytes	Equilibrium Phase
$Li_{10}Ge(PS_6)_2$ (LGPS)	GeS_2, P_2S_7, S
$Li_{9.54}Si_{1.74}P_{1.44}S_{11.7}Cl_{0.3}$ (LSPSCl)	P_2S_7, SCl, SiS_2, S
Li_6PS_5Cl (LPSCl)	SCl, P_2S_7, S
$Li_7P_3S_{11}$	P_2S_7, S
Li_3PS_4	P_2S_7, S

Table S2. Phase equilibriums of chemical and electrochemical reaction between LCO and Li_3PS_4.

Reaction type	State of LCO	Phase equilibrium between LCO and Li_3PS_4
Chemical reaction	fully lithiated	$0.03\ Li_3PS_4 + 0.97\ LiCoO_2 \rightarrow 0.03\ Li_3PO_4 + 0.073\ Li_{10}Co_4O_9 + 0.679\ CoO + 0.121\ Li_2SO_4$
		$0.189\ Li_3PS_4 + 0.811\ LiCoO_2 \rightarrow 0.08\ Co_9S_8 + 0.095\ Li_6CoO_4 + 0.189\ Li_3PO_4 + 0.121\ Li_2SO_4$
		$0.207\ Li_3PS_4 + 0.793\ LiCoO_2 \rightarrow 0.088\ Co_9S_8 + 0.207\ Li_3PO_4 + 0.121\ Li_2SO_4 + 0.275\ Li_2O$
		$0.258\ Li_3PS_4 + 0.742\ LiCoO_2 \rightarrow 0.082\ Co_9S_8 + 0.258\ Li_3PO_4 + 0.113\ Li_2SO_4 + 0.258\ Li_2S$
		$0.314\ Li_3PS_4 + 0.686\ LiCoO_2 \rightarrow 0.314\ Li_3PO_4 + 0.029\ Li_2SO_4 + 0.229\ Co_3S_4 + 0.314\ Li_2S$
		$0.333\ Li_3PS_4 + 0.667\ LiCoO_2 \rightarrow 0.167\ CoS_2 + 0.333\ Li_3PO_4 + 0.167\ Co_3S_4 + 0.333\ Li_2S$
	half lithiated	$0.022\ Li_3PS_4 + 0.978\ Li_{0.5}Co_1O_2 \rightarrow 0.311\ LiCoO_2 + 0.222\ Co_3O_4 + 0.022\ Li_3PO_4 + 0.089\ Li_2SO_4$
		$0.04\ Li_3PS_4 + 0.96\ Li_{0.5}Co_1O_2 \rightarrow 0.16\ LiCoO_2 + 0.04\ Li_3PO_4 + 0.8\ CoO + 0.16\ Li_2SO_4$
		$0.045\ Li_3PS_4 + 0.955\ Li_{0.5}Co_1O_2 \rightarrow 0.045\ Li_3PO_4 + 0.012\ Li_{10}Co_4O_9 + 0.907\ CoO + 0.179\ Li_2SO_4$
		$0.215\ Li_3PS_4 + 0.785\ Li_{0.5}Co_1O_2 \rightarrow 0.086\ Co_9S_8 + 0.009\ Li_6CoO_4 + 0.215\ Li_3PO_4 + 0.169\ Li_2SO_4$
		$0.216\ Li_3PS_4 + 0.784\ Li_{0.5}Co_1O_2 \rightarrow 0.087\ Co_9S_8 + 0.216\ Li_3PO_4 + 0.169\ Li_2SO_4 + 0.027\ Li_2O$
		$0.222\ Li_3PS_4 + 0.778\ Li_{0.5}Co_1O_2 \rightarrow 0.086\ Co_9S_8 + 0.222\ Li_3PO_4 + 0.168\ Li_2SO_4 + 0.027\ Li_2S$
		$0.284\ Li_3PS_4 + 0.716\ Li_{0.5}Co_1O_2 \rightarrow 0.284\ Li_3PO_4 + 0.075\ Li_2SO_4 + 0.239\ Co_3S_4 + 0.104\ Li_2S$
		$0.333\ Li_3PS_4 + 0.667\ Li_{0.5}Co_1O_2 \rightarrow 0.417\ CoS_2 + 0.333\ Li_3PO_4 + 0.083\ Co_3S_4 + 0.167\ Li_2S$
Electrochemical reaction	2.03 V	$0.048\ Li_3PS_4 + 0.952\ LiCoO_2 \rightarrow 0.571\ Li + 0.952\ CoO + 0.19\ Li_2SO_4 + 0.048\ Li_3PO_4$
		$0.217\ Li_3PS_4 + 0.783\ LiCoO_2 \rightarrow 0.435\ Li + 0.087\ Co_9S_8 + 0.174\ Li_2SO_4 + 0.217\ Li_3PO_4$
		$0.268\ Li_3PS_4 + 0.732\ LiCoO_2 \rightarrow 0.537\ Li + 0.244\ Co_3S_4 + 0.098\ Li_2SO_4 + 0.268\ Li_3PO_4$
		$0.333\ Li_3PS_4 + 0.667\ LiCoO_2 \rightarrow 0.667\ Li + 0.667\ CoS_2 + 0.333\ Li_3PO_4$
	4.07 V	$0.032\ Li_3PS_4 + 0.968\ Li_{0.5}CoO_2 \rightarrow 0.294\ Li + 0.041\ Co_{23}O_{32} + 0.032\ LiCoPO_4 + 0.127\ Li_2SO_4$
		$0.033\ Li_3PS_4 + 0.967\ Li_{0.5}CoO_2 \rightarrow 0.319\ Li + 0.016\ Co_3(PO4)_2 + 0.04\ Co_{23}O_{32} + 0.131\ Li_2SO_4$
		$0.039\ Li_3PS_4 + 0.961\ Li_{0.5}CoO_2 \rightarrow 0.442\ Li + 0.077\ Li2Co(SO_4)_2 + 0.019\ Co_3(PO_4)_2 + 0.036\ Co_{23}O_{32}$
		$0.047\ Li_3PS_4 + 0.953\ Li_{0.5}CoO_2 \rightarrow 0.617\ Li + 0.023\ Co_3(PO_4)_2 + 0.03\ Co_{23}O_{32} + 0.188\ CoSO_4$
		$0.05\ Li_3PS_4 + 0.95\ Li_{0.5}CoO_2 \rightarrow 0.625\ Li + 0.025\ Co_3(PO_4)_2 + 0.225\ Co_3O_4 + 0.2\ CoSO_4$
		$0.065\ Li_3PS_4 + 0.935\ Li_{0.5}CoO_2 \rightarrow 0.661\ Li + 0.032\ Co_3(PO_4)_2 + 0.581\ CoO + 0.258\ CoSO_4$
		$0.148\ Li_3PS_4 + 0.852\ Li_{0.5}CoO_2 \rightarrow 0.87\ Li + 0.074\ Co_3(PO_4)_2 + 0.039\ Co_9S_8 + 0.278\ CoSO_4$
		$0.171\ Li_3PS_4 + 0.829\ Li_{0.5}CoO_2 \rightarrow 0.927\ Li + 0.085\ Co_3(PO_4)_2 + 0.11\ Co_3S_4 + 0.244\ CoSO_4$
		$0.2\ Li_3PS_4 + 0.8\ Li_{0.5}CoO_2 \rightarrow Li + 0.1\ Co_3(PO_4)_2 + 0.3\ CoS_2 + 0.2\ CoSO_4$
		$0.226\ Li_3PS_4 + 0.774\ Li_{0.5}CoO_2 \rightarrow 1.066\ Li + 0.113\ Co_2P_2O_7 + 0.358\ CoS_2 + 0.189\ CoSO_4$
		$0.346\ Li_3PS_4 + 0.654\ Li_{0.5}CoO_2 \rightarrow 1.365\ Li + 0.173\ Co_2P_2O_7 + 0.308\ CoS_2 + 0.096\ S_8O$
		$0.404\ Li_3PS_4 + 0.596\ Li_{0.5}CoO_2 \rightarrow 1.511\ Li + 0.494\ CoS_2 + 0.079\ S_8O + 0.101\ CoP_4O_{11}$
		$0.973\ Li_3PS_4 + 0.027\ Li_{0.5}CoO_2 \rightarrow 2.932\ Li + 0.027\ CoS_2 + 0.054\ S_8O + 0.486\ P_2S_7$

Table S3. Kohn-Sham band gap of compounds formed in the phase equilibrium between $LiCoO_2$ and Li_3PS_4/Li_6PS_5Cl.

Species	Source	Band Gap / eV
Co_9S_8	mp-1513	0
Co_3S_4	mp-943	0
CoS_2	mp-2070	0
$Co_{23}O_{32}$	mp-705564	0
P_2S_7	mp-1006118	2.023
S_8O	mp-27465	2.424
CoO	mp-22408	0.843
Li_2S	mp-1153	3.538
Li_2O	mp-1960	4.992
$CoSO_4$	mp-19379	2.167
Li_2SO_4	mp-558382	6.22
$Li_{10}Co_4O_9$	mp-773128	1.401
Li_6CoO_4	mp-18925	1.964
$Co_3(PO_4)_2$	mp-19264	2.9
Li_3PO_4	mp-13725	5.838
$Co_2P_2O_7$	mp-550468	2.088
CoP_4O_{11}	mp-759681	3.174
LiCl	mp-22905	6.395
$LiClO_4$	mp-30301	5.774
ClO_2	mp-23207	0.966
Co_2PClO_4	mp-622183	2.632
SCl	mp-28096	2.981
PCl_3O	mp-27277	4.684

Table S4. phase equilibriums of chemical and electrochemical reaction between LCO and Li_6PS_5Cl.

Reaction type	State of LCO	Phase equilibrium between LCO and Li_6PS_5Cl
Chemical reaction	fully lithiated	0.024 Li_6PS_5Cl + 0.976 $LiCoO_2$ → 0.078 $Li_{10}Co_4O_9$ + 0.024 Li_3PO_4 + 0.122 Li_2SO_4 + 0.663 CoO + 0.024 LiCl
		0.15 Li_6PS_5Cl + 0.85 $LiCoO_2$ → 0.15 Li_6CoO_4 + 0.15 Li_3PO_4 + 0.078 Co_9S_8 + 0.126 Li_2SO_4 + 0.15 LiCl
		0.172 Li_6PS_5Cl + 0.828 $LiCoO_2$ → 0.46 Li_2O + 0.172 Li_3PO_4 + 0.092 Co_9S_8 + 0.126 Li_2SO_4 + 0.172 LiCl
		0.258 Li_6PS_5Cl + 0.742 $LiCoO_2$ → 0.258 Li_3PO_4 + 0.515 Li_2S + 0.082 Co_9S_8 + 0.113 Li_2SO_4 + 0.258 LiCl
		0.314 Li_6PS_5Cl + 0.686 $LiCoO_2$ → 0.314 Li_3PO_4 + 0.629 Li_2S + 0.029 Li_2SO_4 + 0.229 Co_3S_4 + 0.314 LiCl
		0.333 Li_6PS_5Cl + 0.667 $LiCoO_2$ → 0.333 Li_3PO_4 + 0.667 Li_2S + 0.333 Co_2S_3 + 0.333 LiCl
		0.018 Li_6PS_5Cl + 0.982 $Li_{0.5}Co_1O_2$ → 0.351 $LiCoO_2$ + 0.211 Co_3O_4 + 0.018 Li_3PO_4 + 0.088 Li_2SO_4 + 0.018 LiCl
		0.03 Li_6PS_5Cl + 0.97 $Li_{0.5}Co_1O_2$ → 0.242 $LiCoO_2$ + 0.03 Li_3PO_4 + 0.152 Li_2SO_4 + 0.727 CoO + 0.03 LiCl
	half lithiated	0.036 Li_6PS_5Cl + 0.964 $Li_{0.5}Co_1O_2$ → 0.019 $Li_{10}Co_4O_9$ + 0.036 Li_3PO_4 + 0.181 Li_2SO_4 + 0.887 CoO + 0.036 LiCl
		0.171 Li6PS5Cl + 0.829 $Li_{0.5}Co_1O_2$ → 0.067 Li_6CoO_4 + 0.171 Li_3PO_4 + 0.085 Co_9S_8 + 0.177 Li_2SO_4 + 0.171 LiCl
		0.181 Li_6PS_5Cl + 0.819 $Li_{0.5}Co_1O_2$ → 0.209 Li_2O + 0.181 Li_3PO_4 + 0.091 Co_9S_8 + 0.176 Li_2SO_4 + 0.181 LiCl
		0.222 Li_6PS_5Cl + 0.778 $Li_{0.5}Co_1O_2$ → 0.222 Li_3PO_4 + 0.249 Li_2S + 0.086 Co_9S_8 + 0.168 Li_2SO_4 + 0.222 LiCl
		0.284 Li_6PS_5Cl + 0.716 $Li_{0.5}Co_1O_2$ → 0.284 Li_3PO_4 + 0.388 Li_2S + 0.075 Li_2SO_4 + 0.239 Co_3S_4 + 0.284 LiCl
		0.304 Li_6PS_5Cl + 0.696 $Li_{0.5}Co_1O_2$→ 0.304 Li_3PO_4 + 0.435 Li_2S + 0.348 Co_2S_3 + 0.043 Li_2SO_4 + 0.304 LiCl
		0.333 Li_6PS_5Cl + 0.667 $Li_{0.5}Co_1O_2$ → 0.333 CoS_2 + 0.333 Li_3PO_4 + 0.5 Li_2S + 0.167 Co_2S_3 + 0.333 LiCl
Electrochemical reaction	2.03 V	0.04 Li_6PS_5Cl + $LiCoO_2$ → 0.64 Li + 0.96 CoO + 0.2 Li_2SO_4 + 0.04 Li_3PO_4 + 0.04 LiCl
		0.188 Li_6PS_5Cl + 0.812 $LiCoO_2$ → 0.752 Li + 0.09 Co_9S_8 + 0.218 Li_2SO_4 + 0.188 Li_3PO_4 + 0.188 LiCl
		0.234 Li_6PS_5Cl + 0.766 $LiCoO_2$ → 0.936 Li + 0.255 Co_3S_4 + 0.149 Li_2SO_4 + 0.234 Li_3PO_4 + 0.234 LiCl
		0.25 Li_6PS_5Cl + 0.75 $LiCoO_2$ → Li + 0.375 Co_2S_3 + 0.125 Li_2SO_4 + 0.25 Li_3PO_4 + 0.25 LiCl
		0.333 Li_6PS_5Cl + 0.667 $LiCoO_2$ → 0.333 Co_2S_3 + 0.667 Li_2S + 0.333 Li_3PO_4 + 0.333 LiCl
	4.07 V	0.033 Li_6PS_5Cl + 0.967 $Li_{0.5}CoO_2$ → 0.65 Li + 0.017 $Co_3(PO4)_2$ + 0.167 $CoSO_4$ + 0.033 $LiClO_4$ + 0.25 Co_3O_4
		0.037 Li_6PS_5Cl + 0.963 $Li_{0.5}CoO_2$ → 0.704 Li + 0.019 $Co_3(PO_4)_2$ + 0.185 $CoSO_4$ + 0.037 ClO2 + 0.241 Co3O4
		0.043 Li_6PS_5Cl + 0.957 $Li_{0.5}CoO_2$ → 0.739 Li + 0.217 $CoSO_4$ + 0.043 Co_2PClO_4 + 0.217 Co_3O_4
		0.056 Li_6PS_5Cl + 0.944 $Li_{0.5}CoO_2$ → 0.806 Li + 0.556 CoO + 0.278 $CoSO_4$ + 0.056 Co_2PClO_4
		0.121 Li_6PS_5Cl + 0.879 $Li_{0.5}CoO_2$ → 1.163 Li + 0.035 Co_9S_8 + 0.319 $CoSO_4$ + 0.121 Co_2PClO_4
		0.137 Li_6PS_5Cl + 0.863 $Li_{0.5}CoO_2$ → 1.255 Li + 0.294 $CoSO_4$ + 0.137 Co_2PClO_4 + 0.098 Co_3S_4
		0.143 Li_6PS_5Cl + 0.857 $Li_{0.5}CoO_2$ → 1.286 Li + 0.143 Co_2S_3 + 0.286 $CoSO_4$ + 0.143 Co_2PClO_4
		0.158 Li_6PS_5Cl + 0.842 $Li_{0.5}CoO_2$ → 1.368 Li + 0.263 CoS_2 + 0.263 $CoSO_4$ + 0.158 Co_2PClO_4
		0.305 Li_6PS_5Cl + 0.695 $Li_{0.5}CoO_2$ → 2.178 Li + 0.085 CoS_2 + 0.305 Co_2PClO_4 + 0.169 S_8O
		0.404 Li_6PS_5Cl + 0.596 $Li_{0.5}CoO_2$ → 2.725 Li + 0.101 CoP_4O_{11} + 0.494 CoS_2 + 0.079 S_8O + 0.404 SCl
		0.443 Li_6PS_5Cl + 0.557 $Li_{0.5}CoO_2$ → 2.934 Li + 0.074 CoP_4O_{11} + 0.484 CoS_2 + 0.156 S_8O + 0.148 PCl_3O
		0.771 Li_6PS_5Cl + 0.229 $Li_{0.5}CoO_2$ → 4.743 Li + 0.229 CoS_2 + 0.257 P_2S_7 + 0.2 S_8O + 0.257 PCl_3O
		0.871 Li_6PS_5Cl + 0.129 $Li_{0.5}CoO_2$ → 5.29 Li + 0.129 CoS_2 + 0.29 P_2S_7 + 0.29 PCl_3 + 0.258 S_8O
		0.973 Li_6PS_5Cl + 0.027 $Li_{0.5}CoO_2$ → 5.851 Li + 0.027 CoS_2 + 0.486 P_2S_7 + 0.054 S_8O + 0.973 SCl

Table S5. Comparation of battery performance of cells assembled with different SSEs and cathode in sulfide-based ASSBs.

No.	Cathode	SSEs	Temp (°C)	Discharge compacity (mAh g-1)	Capacity retention (%)	Ref.
1	$LiNi_{0.8}Co_{0.1}Mn_{0.1}O_2$	β-Li_3PS_4	25 ℃	124 (0.1 C)	65.3 (0.1C, 50 cycles)	[15]
2	$LiNi_{0.8}Co_{0.1}Mn_{0.1}O_2$	β-Li_3PS_4	25 ℃	127 (0.1 C)	78.7 (0.1C, 25 cycles)	[16]
3	$LiNi_{0.8}Co_{0.1}Mn_{0.1}O_2$	LiGePS	35 ℃	155.4 (0.1 C)	50.1 (0.3C, 100 cycles)	[17]
4	$LiNi_{0.8}Co_{0.1}Mn_{0.1}O_2$	Li_6PS_5Cl	RT	159 (0.1 C)	90 (0.1C, 600 cycles)	[18]
5	$LiNi_{0.83}Mn_{0.06}Co_{0.11}O_2$	Li_6PS_5Cl	30 ℃	204(0.2 C)	/	[19]
6	$LiNi_{0.88}Co_{0.09}Mn_{0.03}O_2$	Li_6PS_5Cl	33 ℃	200.7 (0.1 C)	86.5 (1C, 500 cycles)	[20]
7	$LiNi_{0.6}Co_{0.2}Mn_{0.2}O_2$	β-Li_3PS_4	25 ℃	123 (0.1 C)	/	[21]
8	$LiNi_{0.6}Co_{0.2}Mn_{0.2}O_2$	β-Li_3PS_4	25 ℃	106 (0.1 C)	64 (0.1C, 100 cycles)	[22]
9	$LiNi_{0.6}Co_{0.2}Mn_{0.2}O_2$	Li_6PS_5Cl	RT	141(0.05 C)	97 (0.05C, 20 cycles)	[23]
10	$LiNi_{0.6}Co_{0.2}Mn_{0.2}O_2$	Li_6PS_5Cl	30 ℃	155 (0.1 C)	/	[24]
11	$LiNi_{0.6}Co_{0.2}Mn_{0.2}O_2$	Li_6PS_5Cl	45 ℃	161 (0.2 C)	45.5 (0.2C, 200 cycles)	[25]
12	$LiNi_{0.5}Mn_{1.5}O_4$	LGPS	25 ℃	80 (0.05 C)	70.1 (0.05 C, 10 cycles)	[26]
13	$LiNi_{0.5}Mn_{1.5}O_4$	Li_6PS_5Cl	30 ℃	83.4 (0.1 C)	70(0.1 C, 100 cycles)	[27]
14	$LiMn_2O_4$	Li_6PS_5Cl	/	73 (0.1 C)	96 (0.1 C, 22 cycles)	[28]
15	$LiCoO_2$	LGPS	30 ℃	119(0.1 C)	55(0.1 C, 300 cycles)	[29]
16	$LiCoO_2$	LGPS	/	102(0.1 C)	80(0.1 C, 100 cycles)	[30]
17	$LiCoO_2$	β-Li_3PS_4	25 ℃	82	97.56(10 cycles)	[31]
18	$LiCoO_2$	Li_6PS_5Cl	30 ℃	119.6(0.05 C)	/	[32]
19	$LiCoO_2$	Li_6PS_5Cl	30 ℃	118 (0.2 C)	88.8(0.2 C, 50 cycles)	[33]
20	$LiCoO_2$	Li_6PS_5Cl	30 ℃	125.9 (0.2 C)	74.74(0.2 C, 100 cycles)	[34]
21	Li_2RuO_3	β-Li_3PS_4	100 ℃	220 (0.07 C)	76 (0.07 C, 95 cycles)	[35]
22	Li_2RuO_3	Li_6PS_5Cl	RT	257 (0.05C)	90 (1 C, 1000 cycle)	[36]

Table S6. Numbers and percentages of compounds for each category that pass each filter of the screening.

Filter	Polyanionic oxides	Halides	Non-polyanionic oxides	Total
2[a]	587 (10.4%)	231 (21.0%)	377 (9.4%)	1195
3[b]	203 (34.6%)	130 (56.3%)	151 (40.1%)	484
4[c]	120 (59.1%)	96 (73.8%)	14 (9.3%)	230
5[d]	25 (20.8%)	21 (21.9%)	2 (14.3%)	48

[a]Phase stability screening.

[b]Exclude the elements trend to form electronically conductive products (Ni, Co, Mn, Ti, V, Fe, Cu…).

[c]Chemical stability screening $\Delta E_{D,mutual}$ ≥ -0.165 eV/atom with Li_6PS_5Cl and NCM.

[d]CVAD+BVSE < 0.6 eV.

Table S7. List of 48 compounds that pass ionic conductivity screening (filter 5).

$\Delta E_{D,mutual}$ is the reaction energy of the specific material with Li_6PS_5Cl and fully lithiated NCM/LCO in eV/atom.

TR is the threshold size of the compounds along a, b, and c direction /Å.

BVSE is the diffusion energy barrier of the material in 1D, 2D, and 3D /eV.

Compounds	$\Delta E_{D,mutual}$			TR			BVSE		
	LPSCl	NCM	LCO	a	b	c	1D	2D	3D
Li_2ZnSiO_4	-0.151	0.000	0.000	0.68	0.64	0.68	0.59	0.59	0.64
$LiTaSiO_5$	-0.067	-0.055	-0.006	0.74	0.74	0.74	0.35	0.35	1.26
$Li_4Al_3Si_3O_{12}Cl$	0.000	-0.053	0.000	0.65	0.65	0.65	0.49	0.49	0.49
Li_3PO_4	0.000	0.000	0.000	0.64	0.60	0.62	0.55	0.55	1.04
$Li_3In_2(PO_4)_3$	-0.155	-0.083	-0.037	0.69	0.86	0.69	0.56	0.60	0.63
$LiBi(PO_3)_4$	-0.152	-0.127	-0.093	0.95	0.92	0.95	0.56	0.56	0.92
$Li_3Sc_2(PO_4)_3$	-0.085	-0.068	-0.020	0.66	0.68	0.72	0.45	0.54	0.61
$LiZr_2(PO_4)_3$	-0.093	-0.086	-0.034	0.91	0.91	0.91	0.56	0.56	0.56
$Li_4P_2O_7$	-0.072	-0.074	-0.040	0.75	0.75	0.75	0.28	0.49	0.49
$LiInP_2O_7$	-0.15	-0.098	-0.052	0.91	0.81	0.58	0.53	0.59	1.16
$LiScP_2O_7$	-0.098	-0.09	-0.044	0.92	0.88	0.60	0.43	0.54	1.07
$Li_4Be_3P_3O_{12}Cl$	-0.064	-0.067	-0.030	0.59	0.59	0.59	0.56	0.56	0.56
$Li_4Be_3P_3O_{12}Br$	-0.063	-0.066	-0.028	0.55	0.55	0.55	0.60	0.60	0.60
$Li_2Mg_2(SO_4)_3$	-0.161	-0.061	-0.049	0.68	0.81	0.68	0.32	0.32	0.55
Li_3BO_3	-0.102	0.000	0.000	0.64	0.61	0.61	0.40	0.49	0.49
$Li_3Sc(BO_3)_2$	-0.086	-0.048	-0.019	0.69	0.69	0.69	0.53	0.53	0.74
$Li_3Bi(BO_3)_2$	-0.161	-0.045	-0.014	0.77	0.78	0.77	0.57	0.60	0.69
$Li_6Nd(BO_3)_3$	-0.089	-0.037	0.000	0.72	0.72	0.69	0.44	0.59	0.94
$Li_6Y(BO_3)_3$	-0.087	-0.038	-0.003	0.68	0.68	0.68	0.43	0.60	0.94
$Li_2Al(BO_2)_5$	0.000	-0.06	-0.041	0.86	0.86	0.86	0.51	0.51	0.56
Li_2AlBO_4	-0.043	-0.047	-0.019	0.69	0.67	0.69	0.26	0.47	1.10
$Li_6B_4O_9$	-0.051	-0.047	-0.015	0.70	0.70	0.70	0.33	0.55	0.55
$Li_{10}B_{14}O_{25}Cl_2$	-0.031	-0.062	-0.057	0.55	0.55	0.55	0.53	0.53	0.53
$Li_2B_3O_4F_3$	-0.070	-0.089	-0.089	0.69	1.08	0.68	0.23	0.59	0.82
$Li_4B_7O_{12}Cl$	0.000	-0.067	-0.066	0.59	0.59	0.57	0.47	0.47	0.47
$LiAuI_4$	-0.110	0.000	0.000	0.50	0.50	0.50	0.32	0.32	0.62
$LiGaI_4$	-0.115	-0.063	-0.040	0.53	0.50	0.48	0.33	0.35	0.35
$LiInI_4$	-0.104	-0.042	0.000	0.60	0.58	0.55	0.36	0.37	0.37
K_2LiAlF_6	-0.087	-0.054	-0.010	1.54	1.54	0.29	0.28	0.28	1.16
Li_2BeF_4	0.000	-0.075	-0.039	0.65	0.65	1.25	0.20	0.20	0.20
Li_2SiF_6	-0.102	-0.122	-0.075	0.58	0.58	0.57	0.46	0.49	0.49
Li_3CrF_6	-0.147	-0.107	-0.066	0.57	0.57	0.60	0.44	0.44	0.53
Li_3ScF_6	-0.085	-0.067	-0.024	0.58	0.58	0.57	0.50	0.52	0.52
Li_4ZrF_8	-0.092	-0.086	-0.040	0.57	0.60	0.57	0.36	0.37	0.40
$LiBF_4$	-0.103	-0.157	-0.144	0.76	0.76	0.84	0.17	0.17	0.17

$Li_3Na_3Al_2F_{12}$	-0.072	-0.058	-0.018	0.61	0.61	0.61	0.22	0.22	0.22
$Li_3Na_3Cr_2F_{12}$	-0.145	-0.079	-0.036	0.62	0.62	0.62	0.22	0.22	0.22
$Li_3Na_3Sc_2F_{12}$	-0.09	-0.055	-0.014	0.63	0.63	0.63	0.25	0.25	0.25
$Li_2RbBe_2F_7$	-0.054	-0.068	-0.031	0.55	0.74	0.55	0.46	0.46	0.91
$LiCsCl_2$	0.000	0.000	0.000	0.55	0.52	0.57	0.43	0.43	0.91
Li_3InCl_6	-0.126	-0.063	-0.014	0.84	0.84	0.84	0.49	0.49	0.49
$LiAlCl_4$	-0.129	-0.156	-0.117	0.64	0.57	0.56	0.30	0.30	0.32
$LiGdCl_4$	-0.120	-0.093	-0.045	0.49	0.49	0.49	0.41	0.41	0.41
Li_3ErBr_6	-0.101	-0.086	-0.046	0.54	0.54	0.48	0.36	0.36	0.45
$LiGaBr_4$	-0.140	-0.081	-0.024	0.62	0.55	0.55	0.33	0.36	0.36
$LiRbBr_2$	0.000	0.000	0.000	0.64	0.45	0.64	0.25	0.53	0.72
Li_3NbO_4	-0.148	0.000	0.000	0.54	0.54	0.54	0.39	0.39	0.39
Li_5TaO_5	-0.132	0.000	0.000	0.52	0.73	0.54	0.51	0.54	1.28

Reference

1. M. A. Green, *J. Appl. Phy.*, 1990, **67**, 2944-2954.
2. V. A. Blatov and A. P. Shevchenko, *Acta Cryst.*, 2003, **59**, 34-44.
3. B. He, A. Ye, S. Chi, P. Mi, Y. Ran, L. Zhang, X. Zou, B. Pu, Q. Zhao, Z. Zou, D. Wang, W. Zhang, J. Zhao, M. Avdeev and S. Shi, *Sci. Data*, 2020, **7**, 153.
4. J. Gao, G. Chu, M. He, S. Zhang, R. Xiao, H. Li and L. Chen, *Science China Physics, Mechanics & Astronomy*, 2014, **57**, 1526-1536.
5. X. He, Q. Bai, Y. Liu, A. M. Nolan, C. Ling and Y. Mo, *Adv. Energy Mater.*, 2019, **9**, 1902078.
6. B. He, S. Chi, A. Ye, P. Mi, L. Zhang, B. Pu, Z. Zou, Y. Ran, Q. Zhao, D. Wang, W. Zhang, J. Zhao, S. Adams, M. Avdeev and S. Shi, *Sci. Data*, 2020, **7**, 151.
7. L. Zhang, B. He, Q. Zhao, Z. Zou, S. Chi, P. Mi, A. Ye, Y. Li, D. Wang, M. Avdeev, S. Adams and S. Shi, *Adv. Funct. Mater.*, 2020, **30**, 2003087.
8. B. He, P. Mi, A. Ye, S. Chi, Y. Jiao, L. Zhang, B. Pu, Z. Zou, W. Zhang, M. Avdeev, S. Adams, J. Zhao and S. Shi, *Acta Materialia*, 2021, **203**, 116490.
9. M. Avdeev, M. Sale, S. Adams and R. P. Rao, *Solid State Ionics*, 2012, **225**, 43-46.
10. Y. Nishitani, S. Adams, K. Ichikawa and T. Tsujita, *Solid State Ionics*, 2018, **315**, 111-115.
11. I. D. Brown and D. Altermatt, *Acta Cryst.*, 1985, **41**, 244-247.
12. S. Adams and J. Swenson, *Phy. Rev. Lett.* 2000, **84**, 4144.
13. S. Adams and J. Stefan, *J. power sources*, 2006, **159**, 200-204.
14. S. Adams and J. Swenson, *J. Phy.: Conden. Matter*, 2005, **17**, S87.
15. R. Koerver, I. Aygün, T. Leichtweiß, C. Dietrich, W. Zhang, J. O. Binder, P. Hartmann, W. G. Zeier and J. Janek, *Chem. Mater.*, 2017, **29**, 5574-5582.
16. R. Koerver, F. Walther, I. Aygün, J. Sann, C. Dietrich, W. G. Zeier and J. Janek, *J. Mater. Chem. A*, 2017, **5**, 22750-22760.
17. X. Li, Q. Sun, Z. Wang, D. Song, H. Zhang, X. Shi, C. Li, L. Zhang and L. Zhu, *J. Power Sources*, 2020, **456**, 227997.
18. Y. Zhang, X. Sun, D. Cao, G. Gao, Z. Yang, H. Zhu and Y. Wang, *Energy Storage Materials*, 2021, **41**, 505-514.
19. C. Doerrer, I. Capone, S. Narayanan, J. Liu, C. R. M. Grovenor, M. Pasta and P. S. Grant, *ACS Appl. Mater. Interfaces*, 2021, **13**, 37809-37815.
20. Y. Wang, Z. Wang, D. Wu, Q. Niu, P. Lu, T. Ma, Y. Su, L. Chen, H. Li and F. Wu, *eScience*, 2022, **2**, 537-545.
21. F. Strauss, T. Bartsch, L. de Biasi, A. Y. Kim, J. Janek, P. Hartmann and T. Brezesinski, *ACS Energy Lett.*, 2018, **3**, 992-996.
22. A. Y. Kim, F. Strauss, T. Bartsch, J. H. Teo, T. Hatsukade, A. Mazilkin, J. Janek, P. Hartmann and T. Brezesinski, *Chemistry of Materials*, 2019, 31, 9664-9672.
23. T. Koç, F. Marchini, G. Rousse, R. Dugas and J.-M. Tarascon, *ACS Appl. Energy Mater.*, 2021, **4**, 13575-13585.
24. Y. J. Nam, D. Y. Oh, S. H. Jung and Y. S. Jung, *Journal of Power Sources*, 2018, **375**, 93-101.
25. F. Walther, F. Strauss, X. Wu, B. Mogwitz, J. Hertle, J. Sann, M. Rohnke, T. Brezesinski and J. Janek, *Chem. Mater.*, 2021, **33**, 2110-2125.
26. G. Oh, M. Hirayama, O. Kwon, K. Suzuki and R. Kanno, *Chem. Mater.*, 2016, **28**, 2634-2640.
27. H. J. Lee, X. Liu, Y. Chart, P. Tang, J. G. Bae, S. Narayanan, J. H. Lee, R. J. Potter, Y. Sun and M. Pasta, *Nano Lett.*, 2022, **22**, 7477-7483.

28. J. r. m. Auvergniot, A. Cassel, J.-B. Ledeuil, V. Vialle, V. Seznec and R. m. Dedryvère, *Chem. Mater.* , 2017, **29**, 3883−3890.
29. W. Zhang, F. H. Richter, S. P. Culver, T. Leichtweiss, J. G. Lozano, C. Dietrich, P. G. Bruce, W. G. Zeier and J. Janek, *ACS Appl. Mater. Interfaces*, 2018, **10**, 22226-22236.
30. W. Zhang, T. Leichtweiss, S. P. Culver, R. Koerver, D. Das, D. A. Weber, W. G. Zeier and J. Janek, *ACS Appl. Mater. Interfaces*, 2017, **9**, 35888-35896.
31. Y. Ito, M. Otoyama, A. Hayashi, T. Ohtomo and M. Tatsumisago, *J. Power Sources*, 2017, **360**, 328-335.
32. L. Wang, R. Xie, B. Chen, X. Yu, J. Ma, C. Li, Z. Hu, X. Sun, C. Xu, S. Dong, T. S. Chan, J. Luo, G. Cui and L. Chen, *Nat. Commun.*, 2020, **11**, 5889.
33. S. H. Jung, K. Oh, Y. J. Nam, D. Y. Oh, P. Brüner, K. Kang and Y. S. Jung, *Chem. Mater.*, 2018, **30**, 8190-8200.
34. L. Wang, X. Sun, J. Ma, B. Chen, C. Li, J. Li, L. Chang, X. Yu, T. S. Chan, Z. Hu, M. Noked and G. Cui, *Adv. Energy Mater.*, 2021, **11**.
35. N. K, N. Y, S. A, A. Hayashi, M. Deguchi, C. Hotehama, H. Tsukasaki, S. Mori, Y. Orikasa, K. Yamamoto, Y. Uchimoto and M. Tatsumisago, *Sci. Adv.*, 2020, **6**, eaax7236.
36. Y. Q. Wu, K. Zhou, F. C. Ren, Y. Ha, Z. T. Liang, X. F. Zheng, Z. Y. Wang, W. Yang, M. J. Zhang, M. Z. Luo, C. Battaglia, W. L. Yang, L. Y. Zhu, Z. L. Gong and Y. Yang, *Energy Environ. Sci.*, 2022, 15, 3470-3482.